2014 IEEE International Conference on Robotics & Automation (ICRA)
Hong Kong Convention and Exhibition Center
May 31 - June 7, 2014. Hong Kong, China

A paper-based electrostatic zipper actuator for printable robots

Abraham Simpson Chen[1], Hongli Zhu[2], Yuanyuan Li[2], Liangbing Hu[2], and Sarah Bergbreiter[1]

***Abstract*— A paper-based electrostatic zipper actuator for printable robotics has been designed, fabricated and characterized. A simple fabrication process that utilizes paper with a carbon nanotube ink is used to create electrodes separated by either a mylar or parylene dielectric layer. A 5 cm x 1 cm actuator demonstrated a maximum static deflection of 1.8 cm and a bandwidth of approximately 12 Hz. Static power dissipation was under 1 μW. Two of these actuators are combined to demonstrate simple motion in a 6 cm x 1 cm x 1 cm robot using assymetric friction with the ground, achieving speeds up to 33 mm/min.**

I. Introduction

Robots that can be printed on paper and folded into their final 3-dimensional shape offer the ability to easily, quickly, and inexpensively create robots with varying designs and functionality. Recent incarnations of these "printable" robots have demonstrated walking, crawling, rolling, and grasping [1], [2], [3], [4], [5]. These robots are not far removed from previous demonstrations in robotic origami in which various shapes could be folded using compliant joints fabricated using the Smart Composite Microstructures (SCM) process [6], [7].

In general, these robots have focused on printing and folding to create robot mechanisms and linkages as opposed to active components like motors and sensors. Some actuators have been integrated to automatically fold printed robots – shape memory alloy [8] and shape memory polymer [3] are two examples. These materials can be integrated with fabrication processes like SCM, which make them compatible with printable robots. Once the robot is folded however (automatically or manually), locomotion is often driven by off-the-shelf electromagnetic actuators like DC motors or servos due to greater efficiency and speed [3], [4], but shape memory alloys are also used [2]. Other work has demonstrated shape memory alloys integrated on printer paper (in contrast to the more expensive polymer materials used more commonly with SCM) to fold and actuate origami structures [9].

Given the goal to quickly and inexpensively create printable robots, it would be ideal if the actuation driving locomotion in these robots could also be printed. It is also advantageous to reduce the power requirements of these actuators (and therefore the requirement for a large battery) while maintaining high speeds for more dynamic robot locomotion. The shape memory alloys and polymers that have been previously demonstrated tend to be slow and power hungry. For this reason, this work is focused on the development of a low-power, high bandwidth, paper-based actuator for printable robotics and robotic origami.

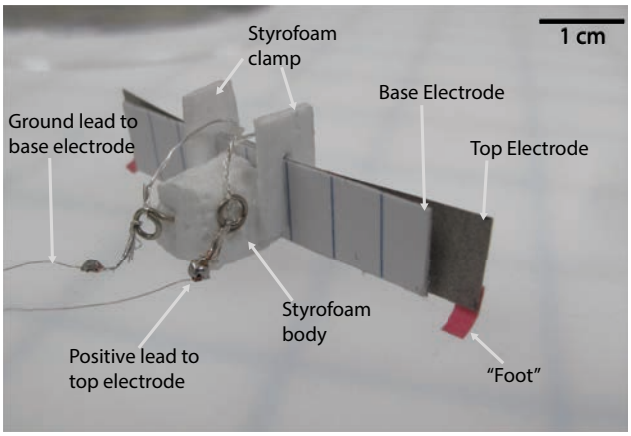

Fig. 1. A 6 cm x 1 cm x 1 cm, 550 mg paper robot. Power and control is provided through tethers and the 'foot' are used to provide asymmetric friction contact with the ground.

A variety of methods can be used to create efficient actuators from 2-dimensional substrates like paper. Moses used a 3-d printer to create a flat electromagnetic motor [10]. Piezoelectrics have been integrated with SCM to create unimorphs with relatively large displacements [11]. Okuzaki used electroactive polymers films in conjunction with folding to design actuators with over 100% strain [12]. Wang demonstrated an electrostatic induction motor using thin sheets of polymer with metal electrodes [13].

The actuator designed and demonstrated in this work will focus on improved efficiency and bandwidth over shape memory materials as well as simplified fabrication through the use of low-cost materials like paper. Electrostatics are chosen due to their material simplicity (typically a conductor and a dielectric) and efficiency. One drawback for the use of electrostatics is the high voltage required (typically several 100 V) even though power requirements are minimal. However, small, low weight power electronics are already in development to drive actuators like these [14], [15].

Instead of metal conductors, this actuator utilizes paper printed with a carbon nanotube (CNT) ink. These CNT-paper conductors have been previously demonstrated using an inkjet-based printing process [16]. Both mylar and parylene dielectrics have been demonstrated, which are compatible with SCM or other robot printing processes. Instead of the

[1]Abraham Simpson Chen and Sarah Bergbreiter are with the Department of Mechanical Engineering and Institute of Systems Research, University of Maryland, College Park, MD 20740, USA abc1@umd.edu

[2]Hongli Zhu and Liangbing Hu are with the Department of Materials Science and Engineering, University of Maryland, College Park, MD 20740, USA

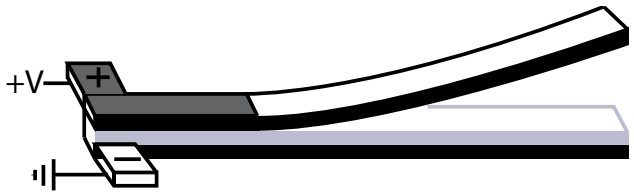

Fig. 2. Schematic of the paper zipper actuator. The top electrode is curled to a set deflection and when the electrodes (black) are stepped up to the pull-in voltage, the top electrode collapses down. The electrodes are separated by the dielectric (gray).

electrostatic induction topology previously shown in [13], the actuator in this paper uses an electrostatic zipper topology common in microelectromechanical systems (MEMS) to achieve large deflections without complex assembly [17].

Section II will describe the design and fabrication of this actuator and the actuator is characterized with respect to its deflection, power requirements, and frequency response in Section III. This actuator is then demonstrated using the tethered robotic device in Fig. 1. The design of this robot along with locmotion results are provided in Section IV.

II. Actuator Design and Fabrication

The primary goals in the design and fabrication of this actuator are in line with the goals of printable robotics: inexpensive materials and a printable design that can easily be folded into shape. Actuator requirements include efficient actuation, linear displacements of millimeters to centimeters, the potential to drive robots at high speeds (multiple body lengths per second), and simple fabrication.

A. Design

Electrostatic zipper actuators are used to achieve large deflections in MEMS actuation [17]. The basic topology is shown in Fig. 2. Two electrodes, shown in black, are separated by a dielectric, shown in gray. One of the electrodes (top in Fig. 2) with a fixed-free boundary condition, is curved at the fixed end and transitions to a straight beam. The other electrode (bottom in Fig. 2) is fixed to a flat surface. When a voltage is applied between the two electrodes, a force is generated between them (proportional to the inverse square of the gap between them). An instability known as "pull-in" causes the electrodes to collapse together once the voltage is higher than a threshold known as the pull-in voltage. Due to the curvature of the top electrode, this instability 'zips' along the interface between the electrodes as the gap between the electrodes reduces in size. This allows for large deflections based on a relatively small actuation voltage.

Pull-in voltage is particularly important for this actuator since this will define the operating voltage of the device. Brenner showed that pull-in voltage can be roughly approximated with Eqn. 1, where E is the Young's modulus of the paper electrode, $\varepsilon_{r,0}$ are the relative and vacuum dielectric constants respectively, δ_0 is the initial deflection of the actuator (largest gap between electrodes), h is the thickness of the paper electrode, and L is the length of the actuator [17].

$$V_{pull-in} \approx (\frac{\pi}{4})^2 \sqrt{\frac{E}{\varepsilon_0 \varepsilon_r} \frac{\delta_0^3 h^3}{12 L^4}} \quad (1)$$

Brenner's model assumes that the initial state of the actuator (before pull-in) is a straight beam with a slope which results in the boundary conditions $\delta(0)=\delta''(0)=0$ and $\delta'(0)=\delta_0$, where δ_0 is the slope of the straight beam. This is an approximation of the device in Fig. 2 which has the boundary conditions $\delta(0)=\delta'(0)=\delta''(0)=0$. An analytical solution to pull-in voltage for a device similar to that in Fig. 2 is challenging, so future work will examine numerical solutions to obtain a better model. With Eqn. 1, assuming $E = 2GPa$, δ = 4 mm, h = 100 μm, L = 5 cm, and ε_r = 2.5, a pull-in voltage of 170 V is expected.

Increased actuator efficiency over previous shape memory alloys and polymer designs is due to the capacitive nature of this actuator. Theoretically, an electrostatic actuator should have zero current draw in steady state, and current only flows when the actuator is being charged or discharged. In practice however, some current leakage will be observed even under static conditions. These actuators also lend themselves to recovery of the charge that was stored on the actuator electrodes when actuated [18].

B. Fabrication

As seen in Fig. 2, the actuator is composed of two electrodes and a dielectric layer. A key attribute of this actuator is that the electrodes are based on paper and a carbon nanotube ink instead of more common materials like metals or silicon. This results in an actuator much more suited to printable robots.

The actuator electrodes were fabricated as shown in Fig. 3. The substrate was printing paper from Boise Aspen with a basis weight of 75 gsm. In Fig. 3A, the paper was placed on a flat surface and 200 μL of a 5 mg/mL aqueous solution of P3 single walled nano tubes (Carbon Solutions, Inc.) was pipetted onto the paper. The solution was then squeegeed onto the paper with a doctor blade as shown in Fig. 3B. The doctor blade used in this case is a metal cylinder that is elevated above the surface of the paper; the blade was elevated by 60 μm to spread the solution. The paper was then sandwiched between soft paper filters and pressed in a manual-operated press (MTI) at room temperature overnight (Fig. 3C). The resulting conductive paper was then manually cut (Fig. 3D) and overlaid with a dielectric layer.

Two types of dielectric materials were used: mylar and parylene C. 10 μm thick mylar was purchased off the shelf, cut to size, and taped over top of the strips of conductive paper. Mylar has a relatively high breakdown voltage of approximately 400 V/μm which means that higher voltages and larger deflections are possible with this dielectric layer. Parylene C has a lower breakdown voltage but is instead deposited onto the surface of the paper actuator in a batch process (versus manual assembly with mylar) using a Parylene Deposition System Model 2010 from SCS. This is a room temperature, conformal deposition process. In fact,

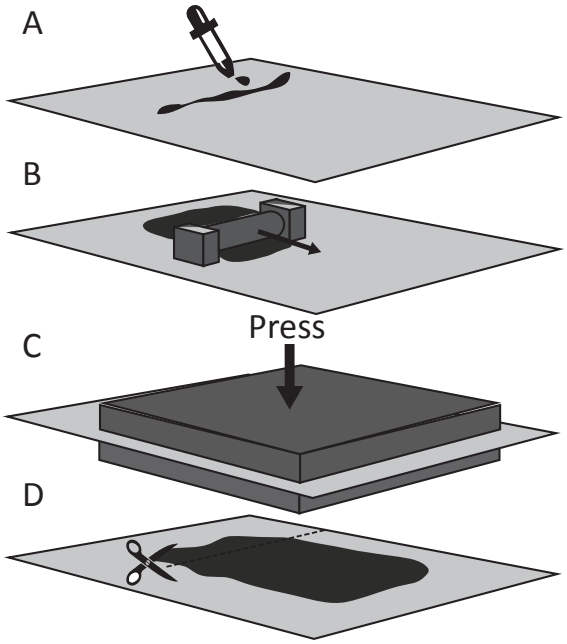

Fig. 3. Fabrication process of conductive paper. A) First 200 μL of CNT solution with a concentration of 5 mg/mL is pipitted onto the paper. B) Using a doctor blade (a metal cylinder elevated at a set height of 60 μm) the CNT solution is spread over the paper. C) The paper is then pressed in a press from (MTI) at room temperature overnight. D) The conductive paper is then manually cut into 5 cm x 1 cm strips.

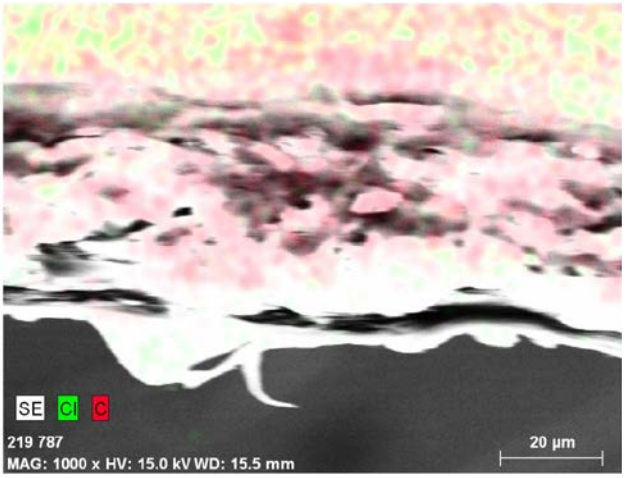

Fig. 4. Field emission scanning electron microscope (FESEM) image showing Chlorine concentration in the cross-section of the conductive paper implying that parylene is conformally coating the fibers in the paper as well

it was found that parylene not only coats the top surface of the paper, but also penetrates into the paper and coats the cellulose fiber [19]. The image in Fig. 4 of the cross-sectional area of the parylene coated conductive paper shows Chlorine atoms within the paper, which are a component of parylene C's chemical structure. Fig. 4 was taken with a field emission scanning electron microscope (SU-70, Hitachi Inc.) equipped with a energy dispersive X-ray spectrometer (EDS: Xflash6100, Bruker Inc.). A parylene thickness of 3.7 μm was used for the characterization of the actuator at voltages lower than 440 V, while a parylene thickness of 10 μm was used for the robot design.

To make electrical contact to the conductive paper layer, packing tape was used to adhere a strip of aluminum foil onto the surface of the the conductive paper during the parylene deposition. This way voltage can still be applied to the conductive paper after the dielectric is deposited. The curvature of the paper was altered by wrapping it around metal cylinders with diameters of 1.4, 2.2, 2.8, and 3.7 cm.

III. Actuator Results

A. Experimental Setup

The actuator used to characterize pull-in voltage, frequency response, and static current draw was 5 cm long (unclamped length) and 1 cm wide. As seen in Fig. 2, the base electrode was either overlayed with mylar or coated with parylene, and was fixed to a plastic substrate. Parylene thickness used for these tests was 3.7 μm and mylar was 10 μm. The top electrode was clamped down by a 20 g mass in order to ensure minimal gap between the top and bottom electrode. Cylinders with diameters varying between 1.4 cm and 3.7 cm were used to set the initial tip deflection. The electrode's radius of curvature was smallest near the clamped end then transitioned to a straight beam.

Pull-in voltage is a function of actuator geometry, materials, and initial deflection [17]. The same actuator geometry and materials were used for all of the tests, and only the initial deflection due to the curvature of the top electrode was changed. A Keithley model 2420 sourcemeter that supplies voltages up to 1100 V was used to apply voltages to the actuator incrementally until pull-in was reached (i.e. the curved top electrode completely collapses to the bottom electrode). For each test, the pull-in voltage for the initial deflection was measured, and after each test the device was cycled between negative and positive voltages to reduce charging in the dielectric. It was observed that after operating the device at high voltages, charging would reduce the performance of the device [20].

To characterize the frequency response of the actuator, a multi-channel custom-made hardware setup with a maximum output voltage of 250 V was used. For each test, the voltage was cycled 20 times between 0 and 250 V at 4-60 Hz.

Deflections for both tests were captured using a Casio Exilim EX-F1 high speed camera and a MATLAB script was used to automatically capture displacement data from the images using a small marker on the tip of the actuator.

Finally, static current draw was measured using the Keithley 2420 sourcemeter while applying 250 V to pull-in the actuator. This was averaged over four trials.

B. Actuator Results

1) Pull-in voltage: To test the actuator's pull-in voltage for a given initial deflection, the voltage was incrementally stepped up until the pull-in was achieved. Before the pull-in voltage, the deflection of the actuator is small but as soon as the pull-in voltage is reached the actuator immediately collapses to the bottom electrode.

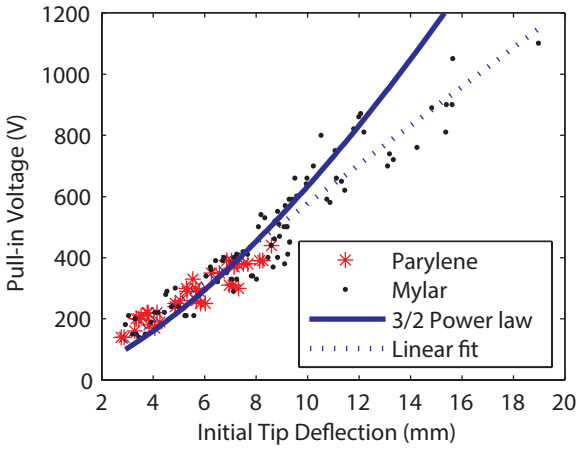

Fig. 5. Pull-in voltage versus initial deflection for 3 devices tested with 10 μm mylar (dots) and 3.7 μm parylene (asterisk) as the dielectric. A 3/2 power law (solid line) and a linear equation (dashed line) was fitted to the mylar.

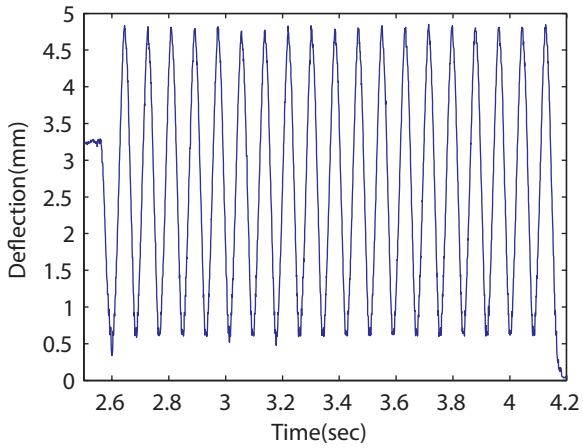

Fig. 6. Time response of paper actuator to a 12 Hz, 250 V signal for 20 cycles with no load

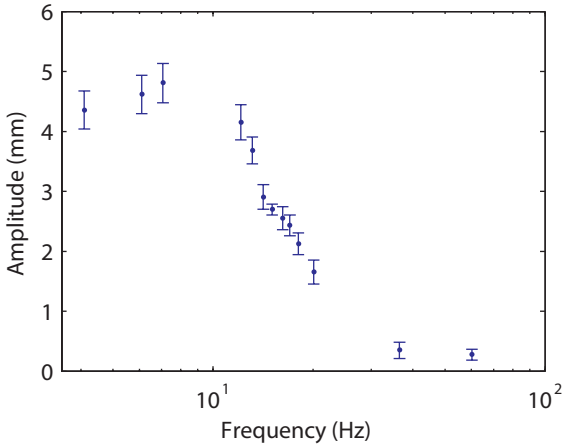

Fig. 7. Frequency response of the paper actuator with no load. Averages of the 20 cycle amplitudes shown in Fig. 6 are taken for each frequency.

Three devices were tested for each type of dielectric: mylar and parylene. The mylar was 10 μm thick and the parylene was 3.7 μm as measured on a glass slide that was placed in the parylene coater with the paper samples. A maximum deflection of 1.8 cm at 1100 V was observed with mylar as the dielectric while a maximum deflection of 8.6 mm at 440 V was observed for parylene. There were no significant differences in performance for devices with parylene or mylar other than the dielectric breakdown of the two materials. The parylene could not achieve the same maximum deflections that were demonstrated with the mylar dielectric because the dielectric began to breakdown and burn the paper at voltages above 440 V.

As seen in Fig. 6, some of the data fits a 3/2 power law, which is expected as $V_{pull-in} \propto \delta_0^{3/2}$ in Eqn. 1. However, some of the data appears to follow a more linear fit. The cause of this discrepancy is still unknown, but one possibility is that charging of the dielectric reduces the pull-in voltage in these instances. In addition, as mentioned previously, Eqn. 1 is an approximation of the experimental device. This approximation could also lead to these discrepancies.

2) Frequency response: Actuator speed is also of importance to printable robots. DC motors and servos are common actuator choices in part because they are faster than shape memory alloy. Fig. 6 shows the actuator tip deflection when driven at a voltage of 250 V with no load applied. Even though the initial deflection is only 3.25 mm, the peak-to-peak deflection amplitude is approximately 4 mm, implying that the actuator is operating at resonance.

This resonant peak is also shown in the frequency response for the actuator (Fig. 7). Error bars represent the standard deviation of deflection amplitude as seen in the raw data in Fig. 6. As expected for a second order system, the roll-off is approximately -40 dB/decade. This data also demonstrates the actuator's ability to move at high speeds; a 4 mm deflection at 12 Hz implies no-load velocities of approximately 5 cm/s.

3) Static Power Draw: Static current draw was measured to provide some idea of power efficiency, although output power of the device was not measured. Over four trials, the static current dissipation was measured at 3.5 nA when the actuator was in its pulled-in state with an applied voltage of 250 V. Despite the high voltages required for these actuators, static power draw is well under 1 μW.

IV. Robot Design and Fabrication

A simple paper robot was designed and built to demonstrate the paper actuator's potential for applications in printable robotics and robotic origami. A basic top-down schematic of the paper robot and its gait is shown in Fig. 8. The robot has two actuators, one on each arm of the robot. These actuators are driven between 0 V and $V_{pull-in}$ to oscillate back and forth. However, this oscillation alone would not move the robot forward. An additional 'foot' on the curved electrode provides asymmetric friction with the ground to drive the robot forward when the actuators

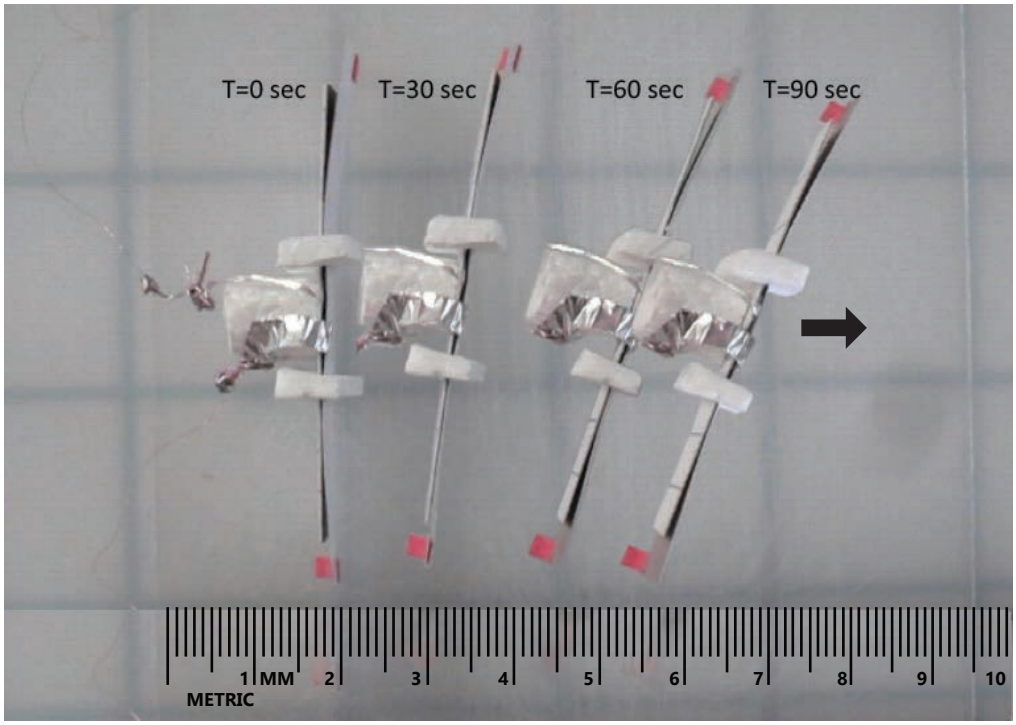

Fig. 9. Motion diagram of paper robot translating 5 cm over a period of 90 seconds. The robot was actuated at approximately 2 Hz at 700 V. Images from the video provided in the supplementary section were overlaid to produce this diagram.

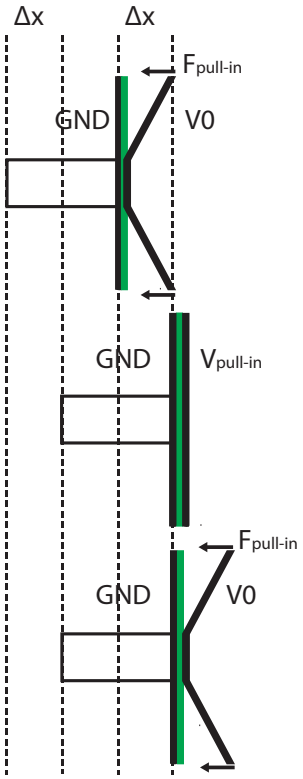

Fig. 8. A top-down view showing the gait and step size for the paper robot. As pull-in voltage is achieved, the robot translates to the right. The base electrode (black) is coated with parylene (green) and fixed, while the top electrode (black) is free to deflect.

pull in. These two actuators can eventually be controlled independently, but are currently tied to a single voltage line.

The main body is made of styrofoam which is attached to the base electrode by double-sided tape. The base electrode is 5 cm long, 1 cm wide, and is taped to a strip of more rigid paper to prevent it from warping when it undergoes the parylene deposition. The base electrode was coated with 10μm thick parylene and is electrically connected to the ground. The top electrode, which is free to deflect, is attached to the base electrode with double-sided tape and curved to form wings on both sides. The top electrode, which is 6 cm long and 1 cm wide, is longer than the base electrode so that it can have a larger deflection while keeping the weight low. Styrofoam clamps are used near the center of the device to keep the electrodes in close contact with each other. 44 gauge wires are used as tethers to supply the voltage to the electrodes.

The final fabricated robot is seen in Fig. 1. The robot is 6 cm x 1 cm x 1 cm with a mass of 550 mg. A plastic substrate was used as a surface for the robot to crawl on and this surface was sanded down to increase friction and the effectiveness of the asymmetric friction feet.

Fig. 9 shows the motion of the paper robot as it translates 55 mm over a period of 2 minutes, achieving a speed of 27.5 mm/min. The robot was actuated at approximately 2 Hz at 700V. The paper robot rotated 67 degrees over time because of uneven friction and uneven actuation between the two wings. In the future, this can be addressed by having two separate wings that are separately actuated to make the robot translate in a straight line or rotate.

V. Conclusions and Future Work

A paper-based electrostatic zipper actuator was designed, fabricated, and characterized. Conductive paper made by painting on a carbon nanotube-based ink was used for the electrodes and both mylar and parylene were tested as dielectric layers. Static deflections up to 1.8 cm were achieved at 1100V with a 5 cm x 1 cm actuator. The bandwidth of this same actuator was measured to be approximately 12 Hz at 250V, and static current draw was 3.5 nA (under 1 μW static power) in its pulled-in state. Using this actuator design, a simple robot was demonstrated translating at speeds up to 33 mm/min.

Future actuator work will focus on optimizing between increasing force and lowering the required voltages for these actuators, along with an improved model to determine pull-in voltages. Stiffer electrodes can increase the force that the actuator can apply, but also increase the required voltage as well. Decreasing dielectric layer thickness using methods like atomic layer deposition (ALD) can increase force with minimal impact on pull-in voltage. New robot designs will also be investigated using this paper actuator including the possibility of more maneuverable robots and self-folding robots.

Acknowledgment

This work is supported in part by the National Science Foundation under Award ECCS1055675. The authors gratefully acknowledge the support of the Maryland NanoCenter and its FabLab.

References

[1] C. D. Onal, R. J. Wood, and D. Rus, "Towards printable robotics: Origami-inspired planar fabrication of three-dimensional mechanisms," in *IEEE International Conference on Robotics and Automation*, Shanghai, May 2011, pp. 4608–4613.

[2] C. Onal, R. Wood, and D. Rus, "An origami-inspired approach to worm robots," *Mechatronics, IEEE/ASME Transactions on*, vol. 18, no. 2, pp. 430–438, April 2013.

[3] S. M. Felton, M. T. Tolley, C. D. Onal, D. Rus, and R. J. Wood, "Robot self-assembly by folding: A printed inchworm robot," in *IEEE International Conference on Robotics and Automation*, Karlsruhe, Germany, May 2013, pp. 277 — 282.

[4] D.-Y. Lee, J.-S. Kim, S.-R. Kim, J.-S. Koh, and K.-J. Cho, "The deformable wheel robot using magic-ball origami structure," in *ASME International Design Engineering and Technical Conferences*, Portland, OR, Aug. 2013.

[5] C. D. Onal, M. T. Tolley, K. Koyanagi, and R. J. Wood, "Shape memory alloy actuation of a folded bio-inspired hexapod," in *IEEE International Conference on Robotics and Automation*, Vilamoura-Algarve, Portugal, Oct. 2012.

[6] E. Hawkes, B. An, N. M. Benbernou, H. Tanaka, S. Kim, E. D. Demaine, D. Rus, and R. J. Wood, "Programmable matter by folding," *Proceedings of the National Academy of Sciences*, vol. 107, no. 28, pp. 12 441–12 445, Jun. 2010.

[7] B. An, N. Benbernou, E. D. Demaine, and D. Rus, "Planning to fold multiple objects from a single self-folding sheet," *Robotica*, vol. 29, no. 01, pp. 87–102, Jan. 2011.

[8] J. K. Paik, E. Hawkes, and R. J. Wood, "A novel low-profile shape memory alloy torsional actuator," *Smart Materials and Structures*, vol. 19, no. 12, p. 125014, Dec. 2010.

[9] J. Qi and L. Buechley, "Animating paper using shape memory alloys." ACM Press, 2012, p. 749.

[10] M. S. Moses and G. S. Chirikjian, "Design of an electromagnetic actuator suitable for production by rapid prototyping," in *ASME International Design Engineering and Technical Conferences*, Washington, DC, Aug. 2011.

[11] J. P. Whitney, P. S. Sreetharan, K. Y. Ma, and R. J. Wood, "Pop-up book MEMS," *Journal of Micromechanics and Microengineering*, vol. 21, no. 11, p. 115021, Nov. 2011.

[12] H. Okuzaki, T. Saido, H. Suzuki, Y. Hara, and H. Yan, "A biomorphic origami actuator fabricated by folding a conducting paper," *Journal of Physics: Conference Series*, vol. 127, p. 012001, Aug. 2008.

[13] H. Wang, A. Yamamoto, and T. Higuchi, "Electrostatic-motor-driven electroadhesive robot," in *Intelligent Robots and Systems (IROS), 2012 IEEE/RSJ International Conference on*, Oct 2012, pp. 914–919.

[14] Y. Tang, C. Chen, A. Khaligh, I. Penskiy, and S. Bergbreiter, "An ultracompact dual-stage converter for driving electrostatic actuators in mobile microrobots," *Power Electronics, IEEE Transactions on*, vol. 29, no. 6, pp. 2991–3000, June 2014.

[15] M. Karpelson, G.-Y. Wei, and R. J. Wood, "Milligram-scale high-voltage power electronics for piezoelectric microrobots," in *Robotics and Automation, 2009. ICRA'09. IEEE International Conference on*. IEEE, 2009, pp. 2217–2224.

[16] L. Hu, D. S. Hecht, and G. Gruner, "Carbon nanotube thin films: Fabrication, properties, and applications," *Chemical Reviews*, vol. 110, no. 10, pp. 5790–5844, Oct. 2010.

[17] M. P. Brenner, J. H. Lang, J. Li, and A. H. Slocum, "Optimal design of an electrostatic zipper actuator," in *Technical Proceedings of the 2004 NSTI Nanotechnology Conference and Trade Show*, vol. 2, 2004, pp. 371–374.

[18] D. Campolo, M. Sitti, and R. Fearing, "Efficient charge recovery method for driving piezoelectric actuators with quasi-square waves," *IEEE Transactions on Ultrasonics, Ferroelectrics and Frequency Control*, vol. 50, no. 3, pp. 237–244, Mar. 2003.

[19] H. Bansa and R. Ishii, "The effect of different strengthening methods on different kinds of paper," *Restaurator*, pp. 51 — 72, 1997.

[20] T.-J. Yao, K. Walsh, and Y.-C. Tai, "Dielectric charging effects on parylene electrostatic actuators," in *Micro Electro Mechanical Systems, 2002. The Fifteenth IEEE International Conference on*. IEEE, 2002, pp. 614–617.